Article:
Wilson, A.J. orcid.org/0000-0002-6602-0990, Davies, C.J., Walker, A.M. et al. (3 more authors) (2025) The formation and evolution of the Earth's inner core. Nature Reviews Earth and Environment, 6. pp. 140-154. ISSN 2662-138X

https://doi.org/10.1038/s43017-024-00639-6

The formation and evolution of Earth's inner core.

Alfred J Wilson[1,*], Christopher J Davies[1], Andrew M Walker[2], Monica Pozzo[3,4], Dario Alfè[3,4,5], and Arwen Deuss[6]

[1]University of Leeds, School of Earth and Environment, Leeds, UK
[2]University of Oxford, Department of Earth Sciences, Oxford, UK
[3]University College London, Department of Earth Sciences, London, UK
[4]University College London, London Centre for Nanotechnology, Thomas Young Centre, London, UK
[5]Universita' di Napoli "Federico II"m Dipartimento di Fisica "Ettore Pancini", Napoli, Italy
[6]Utrecht University, Department of Earth Sciences, Utrecht, Netherlands
[*]e-mail: a.j.wilson1@leeds.ac.uk

ABSTRACT

Growth of the inner core provides crucial power for generating the geomagnetic field and preserves a unique record of deep Earth evolution. The classical picture of inner core growth ignores the fact that the liquid core must have been supercooled below its melting temperature to spontaneously freeze the inner core. In this review we assess the impact of supercooling on inner core formation, growth, dynamics, and the interpretation of seismic and paleomagnetic observations. Mineral physics calculations suggest that a supercooling of at least 450 K is needed to nucleate the inner core, while inferences from geophysical observations constrain the maximum available supercooling to ∼200 K and more likely ∼80 K when satisfying constraints on long-term core-mantle evolution. Supercooling requires that the inner core initially grew rapidly, comparable to the timescale of outer core dynamics, followed by a slower phase of classical equilibrium growth. The rapidly-grown region could have been at least as large as the innermost inner core and is predicted to not convect, with deformation due to heterogeneous inner core growth or coupling to the dynamo-generated magnetic field the most likely explanations of the observed seismic elastic anisotropy. Rapid growth is also expected to produce a signature in the paleomagnetic record.

Key Points

- The iron rich liquids of Earth's core are physically required to be supercooled for the solid inner core to first nucleate but existing thermal history models of core do not consider supercooling of the core prior to inner core growth.
- Supercooled liquid metals are expected to freeze rapidly upon nucleation, perhaps freezing the entire inner core in several years.
- Deformation mechanisms which might be responsible for inner core structure can be modified or negated by supercooling and others are exclusive to this scenario.
- The dynamic consequences and palaeomagnetic signature of a rapidly frozen region in the inner core remain unknown.

1 Introduction

Despite constituting less than 2% of the planet, Earth's inner core (IC) plays a crucial role in the Earth system. As the whole planet loses heat to space, the liquid core cools and the IC grows outward from Earth's centre. Growth arises at the centre because the melting point of the alloy of iron, nickel and lighter elements forming the core increases with depth. At the inner core boundary (ICB) latent heat is released as liquid transforms to solid, providing thermal buoyancy, and lighter elements remain in the liquid because they do not fit into the solid lattice, providing chemical buoyancy[1]. These two effects are the dominant power sources for the geodynamo that generates Earth's magnetic field in the liquid core[2]. Without these power sources the dynamo might have switched off long ago as is suspected for Mars[3]. The geomagnetic field shields Earth from solar radiation and so the presence of the IC is indirectly linked to the surface environment.

The conventional view of Earth's thermal history and IC formation is that the liquid core gradually cooled until the temperature at the centre of the Earth (∼ 6000 K, 360 GPa) met the melting point of the constituent alloy. At that time the solid IC nucleated and began to slowly grow. This growth continued until the present day where the intersection of core temperature and melting temperature is at the seismically observed inner core boundary (ICB, 1221 km from the center of the Earth), which provides the primary constraint on the core's temperature (∼ 5600 K, 330 GPa). This physical model, together with data from

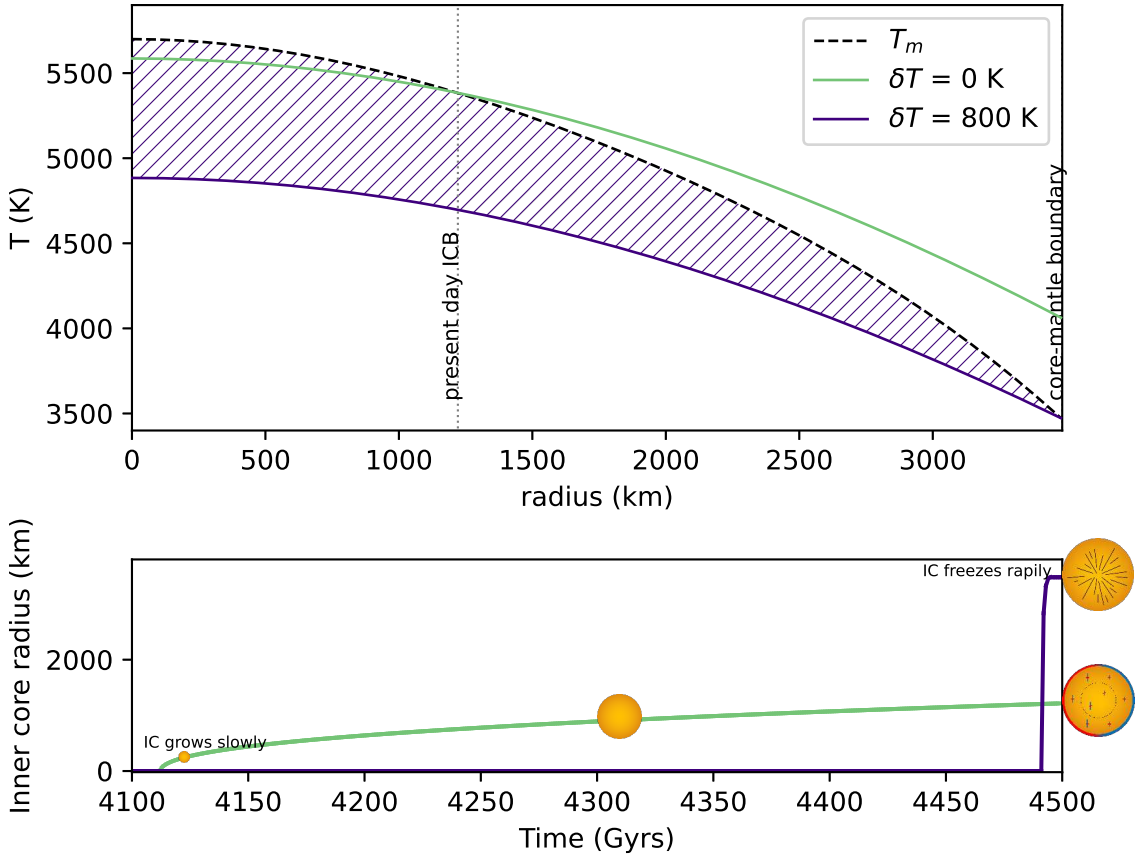

Figure 1. The implications of supercooling on inner core growth. Upper panel) The intersection of core melting temperature (dashed line) and adiabat (solid lines) defines the position of the IC boundary. Supercooling the core far below the melting temperature (purple line) before IC nucleation requires that most of the core was supercooled (hatched area). Lower panel) When the required supercooling to spontaneously nucleate the IC (δT) is achieved, all supercooled liquid will rapidly freeze (section 3). In the purple case (where δT = 800 K is needed to freeze the IC[12, 13, 18]) shown this freezing results in a larger than observed IC, most of which froze in the past 100 Myrs. The green case shows a traditional view where no supercooling is required and the IC grows under a single growth regime. IC: inner core. Supercooling is required to freeze the inner core but large δT is incompatible with observations, meanwhile, the dynamic history of IC growth imprints an observable record in seismological observations of IC structure (section 4).

mineral physics, constrains the thermal structure of the present day core and the balance of heat flux through the Earth. Thermal history models based on this conventional view predict the inner core to be 500 - 1100 Myrs old[4], which depends strongly on the thermal conductivity and composition of the core as well as any additional sources of convective power (for example, light element precipitation[4–7] and radiogenic heating[8,9]).

It has been shown that the conventional view of IC formation and growth, and thus the standard model of the core's thermal history, contain a key flaw: they assume that the inner core formed at the instance when the core temperature T_a fell below its melting temperature T_m at Earth's centre[2, 10, 11] (see Fig 1a). However, homogeneous nucleation (the formation of solid away from pre-existing surfaces) requires the creation of a solid-liquid interface, which comes with an energy cost. This implies that the centre of the core needs to cool below T_m before the inner core nucleates and begins to grow. Estimates of the amount of supercooling (cooling below the melting temperature, sometimes referred to as undercooling and denoted δT) needed make use of Classical Nucleation Theory (CNT, see box 1) together with the extrapolation of lab data[12] or molecular dynamics (MD) simulations of freezing[13] to show that homogeneous nucleation requires a supercooling of 100s of K below T_m before solid crystals form at Earth's centre. Since the core cools at about $\sim$ 100 K Gyrs^{-1}[2, 13] this implies that Earth's inner core should never have formed or that the core is too cold to have any liquid region (Fig. 1). The lack of a physical explanation for the inner core's existence defines the IC nucleation paradox[12].

The effect of supercooling renders all existing models of the core's thermal history incomplete, compromising predictions of the IC age and growth history as well as the resulting links to the paleomagnetic record and seismic observations of the

IC. The existence of the geomagnetic field for at least the last 3.5 Gyrs[14] provides a key constraint on the core's long-term thermal history, while long-term decline followed by rapid increase of the magnetic field strength have been used as an indicator of IC formation[15]. Seismic observations reveal radial variations in wave speed and anisotropy, some of which suggest a distinct innermost inner core, that reflect deformation and texturing processes controlled by the IC growth history. Relating these observations to IC properties and processes requires a coherent model of deep Earth thermal history that incorporates supercooling. Here we first review the available constraints on supercooling from previous mineral physics and geodynamic studies before incorporating viable values into a suite of coupled core-mantle thermal history models. These models allow us to further refine the range of viable supercooling that is consistent with first-order observations of Earth's long-term thermal history: the presence of a long-lived dynamo, the present size of the IC, and the present temperature and heat flux at the top of the convective mantle. A key implication of these models is a period of rapid initial IC growth. We estimate the likely growth rate, its geodynamic implications, and its potential expression in available observations. Finally, we compare the seismically observed structure of the IC and its inferred dynamics with the supercooled thermal histories which have been proposed to produce them before summarising the open questions that remain.

Box 1 - Classical nucleation theory and the inner core nucleation paradox.

The inner core nucleation paradox arises from the way that a liquid transforms to a solid as it cools through its melting temperature. Below the melting temperature the free energy of the solid is lower than the free energy of the same amount of liquid. Although the sign of this energetic term means formation of the solid from the liquid would be favoured, in the absence of pre-existing surfaces some energy is required to form a solid-liquid interface. Until this energy barrier is overcome the liquid state can persist even below the melting point. The size of the barrier decreases as the system is supercooled further below the melting temperature. We observe this effect in the atmosphere where supercooled water droplets persist in the liquid state until snow forms around dust particles or ice flash-freezes on aircraft wings[16]. These examples also illustrate the importance of heterogeneous nucleation, where a pre-existing solid reduces the energy barrier and allows rapid freezing.

Classical nucleation theory (CNT) allows us to describe the way the energy barrier to nucleation evolves with temperature[17]. The key idea is that the difference in chemical potential between solid and liquid $\delta\mu$ is released as energy when the supercooled liquid transforms into a solid. This quantity is proportional to the volume of solid and becomes more favourable as the temperature drops further below the melting temperature. On the other hand, the energy penalty γ associated with the interface is proportional to the interface area and is typically independent of temperature. This penalty means that for any undercooling there is a critical radius for nucleation. The total energy of a homogeneous system ΔG^{hom} decreases if solid particles which are smaller than this radius melt. On the other hand, the total energy of the system decreases if solid particles larger than this radius grow. The energy barrier ΔG^{hom} associated with forming a solid particle of the critical radius r_c is then:

$$\Delta G^{hom} = 4/3\pi r_c^3 \delta\mu + 4\pi r_c^2 \gamma \tag{1}$$

The critical radius gets smaller as the temperature drops. In order to estimate a waiting time τ_w for solidification we imagine that the arrangement of the atoms in the liquid continually fluctuate and that small solid clusters of atoms, with a structure like the solid, continually form and disappear. Nucleation occurs once a cluster larger than the critical radius spontaneously forms (it turns out that the waiting time for this event to occur decreases exponentially with decreasing critical radius) according to:

$$\tau_w = \tau_0 \exp\left(\frac{\Delta G^{hom}(r_c)}{k_B T}\right) \tag{2}$$

where τ_0 is a system specific kinetic pre-factor and k_B is the Boltzmann constant. For traditional thermal history models of the core, the waiting time is long compared to the age of the Earth, even for the vast volume concerned.

2 Nucleation of the Inner Core

Geophysical observations of the deep Earth provide clues as to how much the liquid core might have been supercooled below its melting temperature prior to inner core nucleation. The mechanism by which the inner core might have nucleated provide constraint of the supercooling required to first freeze solids in the liquid core. In this section the supercooling compatible with observations and mineral physics is compared.

2.1 Supercooling of the Earth's core

Estimates of the supercooling required to trigger the nucleation of the inner core can be separated into those which are inferred from geophysical observations, such as the size of the inner core, and those which use mineral physics calculations. The latter

assesses the necessary conditions to overcome the free energy barrier defined by nucleation theory (box 1). Both categories of estimates are summarised in Fig. 2.

Three different approaches have been used to infer the allowed supercooling from geophysical observations. The most direct are derived by tying the core T and melting temperature T_m at the present ICB radius of 1221 km. Assuming that the IC froze in the immediate past requires that the whole IC volume is supercooled with the maximum supercooling arising at Earth's centre[12,13,18–20] (see Fig. S1 of the Supplementary Information). Using a range of T_m and T curves, the maximum δT (the amount of supercooling below the melting temperature) is 420 K[20]. The second approach used geodynamic modelling to argue that trapping < 10 % liquid in the IC (as suggested by Singh[21] using seismic observations) requires that the IC nucleated at no more that half its present size, which limits δT to ~ 100 K. Finally, Pang[22] correlated enhanced seismic scattering in the bottom 420-720 km of the IC with a rapid growth phase; using this radius requires a δT of 25-70 K. Thus, overall geophysical observations constrain the maximum δT in the range 25-420 (Fig. 2).

2.2 Nucleation pathways

Calculations based on mineral physics have also been used to estimate the undercooling required to nucleate solids at Earth's centre via homogeneous and heterogeneous nucleation. The assessment of the supercooling required to homogeneously nucleate the IC began with investigation of pure Fe. Extrapolation of thermodynamic properties[12] at lower P and T, simulations of the freezing process[13] and simulations of nucleation kinetics[18] all suggest that pure Fe requires between 730 K and 1000 K of supercooling to observe a nucleation event in a volume equal to the current IC within 1 Gyrs. Sun et al., 2022[19] found that a metastable BCC phase of pure Fe might provide a favourable route to freezing, needing only 470 K, eventually relaxing to the stable hexagonally close packed (HCP) phase. Other simulations of nucleation have identified defect rich crystal structures[18] indicating that an assumption of CNT, that the most stable phase will be the first to form, is not correct. Although, simulations still predict that large δT is needed and are well described by CNT despite this discrepancy.

The introduction of alloying elements does alter the picture of homogeneous nucleation. Oxygen, Carbon, Silicon and Sulphur are all candidate light elements to be present in the iron-nickel core due to their cosmochemical abundance and partitioning behaviour at core formation conditions. O and C are expected to partition strongly to the liquid iron upon IC freezing[23,24], whilst Si and S partition approximately evenly between solid and liquid[25]. Each of these commonly considered light elements has a distinct effect on the energetics of nucleation. O reduces ΔG^{hom} but also depresses the melting point of the alloy such that the two effects counteract, resulting in a similar degree of supercooling being needed for spontaneous freezing[13]. C has a similar effect on ΔG^{hom} but depresses the melting point of Fe less than O, leading to a reduction in the required supercooling[20]. 5 mol % C in the core reduces the required supercooling in the core to 612($\pm$139) K. However, concentrations this high are difficult to reconcile with partitioning and isotopic data[26] and accretionary modelling[27]. Si and S both have a negative effect on the nucleation barrier[20] and require greater supercooling than the pure case.

Heterogeneous nucleation of iron on a pre-existing surface in the liquid core might offer a marked reduction to the interfacial energy associated with freezing solids. One simple model of heterogeneous nucleation is described by CNT[17] as

$$\Delta G^{het} = f(\theta)\,\Delta G^{hom}, \text{ with } f(\theta) = \frac{2 - 3\cos\theta + \cos^3\theta}{4}, \tag{3}$$

where θ is the wetting or contact angle of the nucleating phase on the pre-existing surface, which reduces the energy barrier ΔG^{hom} by a factor $f(\theta)$(where $\theta \leq 1$). This approximation assumes that the pre-existing surface is flat and that greater affinity of the nucleating phase to this surface is well described by lower wetting angles (where the same volume of nucleated material is spread more thinly over a larger area).

Whilst heterogeneous nucleation provides an attractive solution to the inner core nucleation paradox, its key assumption (the existence of a pre-existing solid facilitating nucleation of the IC at modest supercooling) is difficult to justify. One possibility is that solid material was delivered to the early core from impacted planetesimals; however, this material is not expected to survive melting before reaching the innermost liquid core[12]. A second possibility involves sourcing a metallic phase from subducted mantle material collecting at the CMB. Diamond inclusions suggest that metallic phases are present in the deep mantle[28] and both gold and copper would provide a dense, high melting temperature phase which might sink as diapirs toward the supercooled region of the core. Huguet et al.[12] considered this possibility but concluded that the core would dissolve such a "nugget" before it would reach the centre of the Earth. A final possibility arises from the core's strongly temperature-dependent solubility. Liquid iron is an efficient solvent at the temperatures arising during core formation ($\sim$5000-6000 K)[6,29], but subsequent cooling reduces the solubility of dissolved elements, potentially causing some fraction to precipitate at the coolest region of the outer core. However, this exsolution mechanism is problematic for three reasons: the phase will inevitably be low density compared to the bulk core and so will not easily be mixed into the supercooled region which first forms at the centre of the core; solubility is strongly temperature dependent[4,6,7,9] meaning that precipitates will form at the CMB, furthest from the first supercooled liquids. Furthermore; oxides, which have so far been the most commonly considered precipitates[4,5,7,30], have poor wetting

angles for metals[31] meaning they are unlikely to substantially reduce any nucleation barrier. A resolution to these issues would be a dense metallic phase with a high melting temperature which might either have survived accretion or precipitated at high temperature and pressure. A basic ab initio calculation of the forced dissociation of tungsten (W) and carbon in liquid iron reveals a lower energy configuration when the species are dissolved rather than bonded, eliminating the possibility of a WC phase in the core (see section S2 of the Supplementary Information for details). A more detailed exploration of the potential resolutions to the IC nucleation paradox is given in the section S3 of the Supplementary Information.

Despite the lack of a thermodynamic resolution to the inner core nucleation paradox, the existence of the IC is indisputably established by geophysical observations and so a resolution must be possible. One approach is to search for a mechanism from mineral physics that yields a required supercooling that is compatible with geophysical observations. For example, a smaller required supercooling could lie in a hitherto unidentified difference between core nucleation and the predictions of CNT, the combined effects of multiple light elements, or a novel "dust" that would facilitate nucleation. A second potential resolution arises from noting that nucleation is stochastic and that existing estimates of the required δT to produce the IC do not preclude its existence but instead suggest that nucleation was highly improbable and that the Earth could be a rare case. Whatever the resolution, thermal histories of Earth's deep interior must predict a plausible cooling rate that allows continuous magnetic field generation of the last 3.5 Gyrs and the correct present-day IC size. We now turn to this problem and show that it provides another independent constraint on the viable undercooling.

3 Inner core cooling and crystallisation/growth

A complete model of inner core evolution describes the thermal state of the deep Earth through time. In this section an established model of the coupled core and mantle is described. This model includes adaptations to account for supercooling of the liquid core prior to inner core nucleation and exploration of the inner core growth rate from a supercooled state.

3.1 Inner core growth rate

The existence of a nucleation barrier suggests that the IC has grown under at least two regimes[22,32]: one immediately after a successful nucleation event where all liquid in the supercooled region freezes, and the second the classical picture where the ICB tracks the core melting point (Fig.1). The rate g at which the supercooled region of the liquid core crystallised is not known but is estimated to vary between 0 at T_m (because the driving force $\delta\mu = 0$ at T_m) and a theoretical maximum growth rate g_0 as[33]

$$g = g_0 \left(1 - \exp \frac{-\delta\mu(P,T,x)}{RT}\right), \tag{4}$$

where R is the gas constant and $\delta\mu$ is the difference in chemical potential between the solid and liquid which depends on pressure P, temperature T and composition x. Molecular dynamics simulations[34] suggest that for Ni at ambient pressure g increases as 0.2 m s^{-1} K^{-1} from 0 at T_m. Simulations of binary iron alloy nucleation[20] at IC conditions suggest g = 280 m s^{-1} at 4000 K meaning a gradient of 0.07 m s^{-1} K^{-1}. These estimates agree with experimental results indicating that crystal growth has close to zero activation energy beyond a critical size in supercooled liquids[35]. Such values of g imply a supercooled volume the size of the present day IC would freeze completely in less than one year and perhaps as quickly as hours. This growth rate implies that dendritic crystal growth and liquid inclusions concentrated in impurities are both highly relevant to any rapid growth phase of the IC. Latent heat release and chemical partitioning might decrease the growth rate, as we will discuss later in this section, but g is still expected to be much faster than the ∼Myr timescale for evolution of the well-mixed core (see section 4). In this section we first focus on long-term core-mantle thermal history, where the initial rapid phase of IC growth can be ignored, before returning to consider the growth in the supercooled region.

3.2 A model of inner core nucleation and growth

We use an established thermal history model[36,37] to demonstrate the effects of supercooling on IC growth. This 1D parameterisation of coupled core-mantle evolution uses energy balances to calculate changes in mantle and core temperature over geological time (see Driscoll and Davies, 2023[37,38] and Driscoll and Bercovici, 2014[39] for details) and predicts key deep Earth properties including the IC growth rate, long-term variations of magnetic field intensity, and heat transport. The mantle model is a classic "plate tectonic" parameterisation using boundary layer theory to determine the heat fluxes at the CMB (Q_{cmb}) and out of the convecting mantle, while the core model assumes the usual adiabatic, hydrostatic and chemically well-mixed state. We do not considered the added complexities of a stably stratified layer[37,40], precipitation of oxides[4,30] below the CMB, the influence of a basal magma ocean at the base of the mantle[41,42], or alternative parameterisations of mantle dynamics[43,44]. Traditional thermal history models of the core define the ICB at each time step as the intersection of adiabat and the melting curve, meaning that there is only one (equilibrium) growth regime and no supercooling. Here, we add the nucleation barrier

and corresponding supercooling to these models by requiring that the centre of the core reaches a temperature lower than the melting temperature T_m by a prescribed supercooling value δT before the IC nucleates (see Fig. 1).

The key parameters determining core evolution are its chemical composition, temperature structure, and thermal conductivity. As in previous work[10] three simple compositions are considered: $Fe_{0.82}O_{0.08}Si_{0.10}$, $Fe_{0.79}O_{0.13}Si_{0.08}$ and $Fe_{0.81}O_{0.17}Si_{0.02}$ which correspond respectively to present day ICB density contrasts $\delta\rho$ of 0.6 g cm^{-3}, 0.8 g cm^{-3} and 1.0 g cm^{-3}, matching the range estimated from normal modes[45]. Increasing O concentration increases the power supplied to the dynamo by compositional convection and decreases the melting point of the alloy. We investigated a range of pure iron melting curves[46–48] and focus on the one[46] with the largest value at Earth's centre, which maximises the available supercooling. For the supercooled region we considered two temperature profiles: an adiabat matched to the liquid core's temperature at the ICB and an isothermal profile, where the entire supercooled region assumes the temperature at the ICB (see section S1 of the Supplementary Information for details). The isothermal profile is an extreme case that maximises the actual supercooling that can be achieved and might arise due to an increase in thermal conductivity with depth that leads to stable stratification of the innermost core[49]. We consider core thermal conductivity $k = 30, 50, 70$ W m^{-1} K^{-1} to explore both low and moderately high conductivity scenarios[10,50–52]. The supercooling is varied within the range inferred from geophysical observations (Fig. 2), which is compatible with the assumed core thermal structure. All other parameters remain unchanged from the original model[37]. For each parameter set we tune the initial temperature of the core $T_{cmb}^{4.5Ga}$ and mantle $T_m^{4.5Ga}$ and the ratio of upper to lower mantle viscosity f_{visco} to satisfy 4 constraints: sufficient entropy available for ohmic dissipation such that the geodynamo has been active for the past 3.5 Gyrs[53–57]; the present IC radius of 1221 km; the current mid-mantle temperature of 2320 K[58]; the current heat loss from the convective mantle of 38 TW[59]. We set $T_m^{4.5Ga} = 3400$ K for all cases where $\delta\rho$ = 0.6 or 0.8 g cm^{-3} and 3000 K for $\delta\rho$ = 1.0 g cm^{-3}. We limit $T_{cmb}^{4.5Ga}$ to a maximum value of 7000 K as extreme core temperatures imply a long lived magma ocean. For consistency with prior implementations of this model[37–39], we only vary f_{visco} between 1 and 20.

Fig. 3 displays coupled core-mantle thermal histories for different k, $\delta\rho$ and δT with an adiabatic supercooled region (the isothermal case gives similar results and is presented in the Fig. S3 of the Supplementary Information). The case where $\delta T = 0$ K represents a traditional model and reproduces Figure 10 in Driscoll and Davies[38]. All cases produce a young IC less than 800 Myrs old and a hot early CMB temperature > 4500 K, which exceeds current estimates of the lower mantle melting temperature[60], suggesting the existence of an early molten region above the core (Fig. 3 upper panel). The present day CMB heat flux for solutions presented in Fig. 3 varies with composition and supercooling, with ranges of 9.2-9.9 TW, 9.1-9.2 TW and 8.2-8.4 TW for $\delta\rho$ = 0.6, 0.8 and 1.0 g cm^{-3} respectively. These features are consistent with previous core thermal histories[10,11,61] despite the different model setups that have been employed. The effect of changing core thermal conductivity is not particularly prominent in the figure because this quantity only affects the power available to the dynamo and all values of k tested produce sufficient power at all times; the limiting factor for the success of these models within the parameter space explored is matching the size of the IC at the present day. The maximum supercooling that can be sustained prior to IC nucleation in successful thermal histories is 77 K, although this case also requires that a present day $T_{CMB} = 4360$ K which exceeds estimates of the mantle melting temperature[60], implying an extant basal magma ocean. Indeed all cases where $\delta\rho$ = 0.6 g cm^{-3} fail in this regard. Cases where $\delta\rho$ = 0.8 and 1.0 g cm^{-3} have successful solutions with δT no greater than 60 K. At this upper limit of supercooling, all cases converge on an IC age of 0 and a fast freezing region with radius 1221 km, because they require that the entire IC froze in the immediate past. At modest supercooling (less than 30 K), the IC age differs by up to $\sim$400 Myrs between cases. Models with larger $\delta\rho$ produce an older IC because the enhanced gravitational energy release on freezing slows core cooling.

A range of estimates for changes in seismic anisotropy with depth in the inner core is shown in Fig. 3 where the estimated size of the innermost IC ranges from 300-750 km[62,63]. In order to rapidly freeze this volume, the centre of the Earth must have been cooled by at least 5 K and by no more than 40 K, although this value depends on the composition of the core as $\delta\rho$ = 0.8 and 1.0 g cm^{-3} cases freeze 750 km radius regions with $\delta T \sim 35$ K. Cases which are compatible with an innermost IC which froze rapidly have IC ages between 450 and 750 Myrs.

3.3 Freezing of supercooled Fe liquids

We now return to consider the growth of the supercooled region. Molecular dynamics simulations[9,34] suggest that a volume the size of the IC could have frozen within days but do not consider the influence of latent heat release or partitioning of light elements as the supercooled region grows. Latent heat release could slow the growth rate if the heat is trapped in the supercooled region, thereby increasing the local temperature and decreasing the driving force ($\delta\mu$) for growth, which could occur if thermal conduction and core convection are too slow to transfer heat away from the freezing interface into the bulk core. We consider a simple model of this process that integrates Eq. 4 forward in time using the thermodynamic model of Komabayashi[64] to evaluate $\delta\mu(P,T)$ and the calculated latent heat release to update an initially adiabatic temperature profile (see section S6 of the Supplementary Information for details). When heat transfer is limited by thermal conduction the results show that latent heat release slows the growth time of the supercooled region to $\sim$ 100 years. This value is independent of

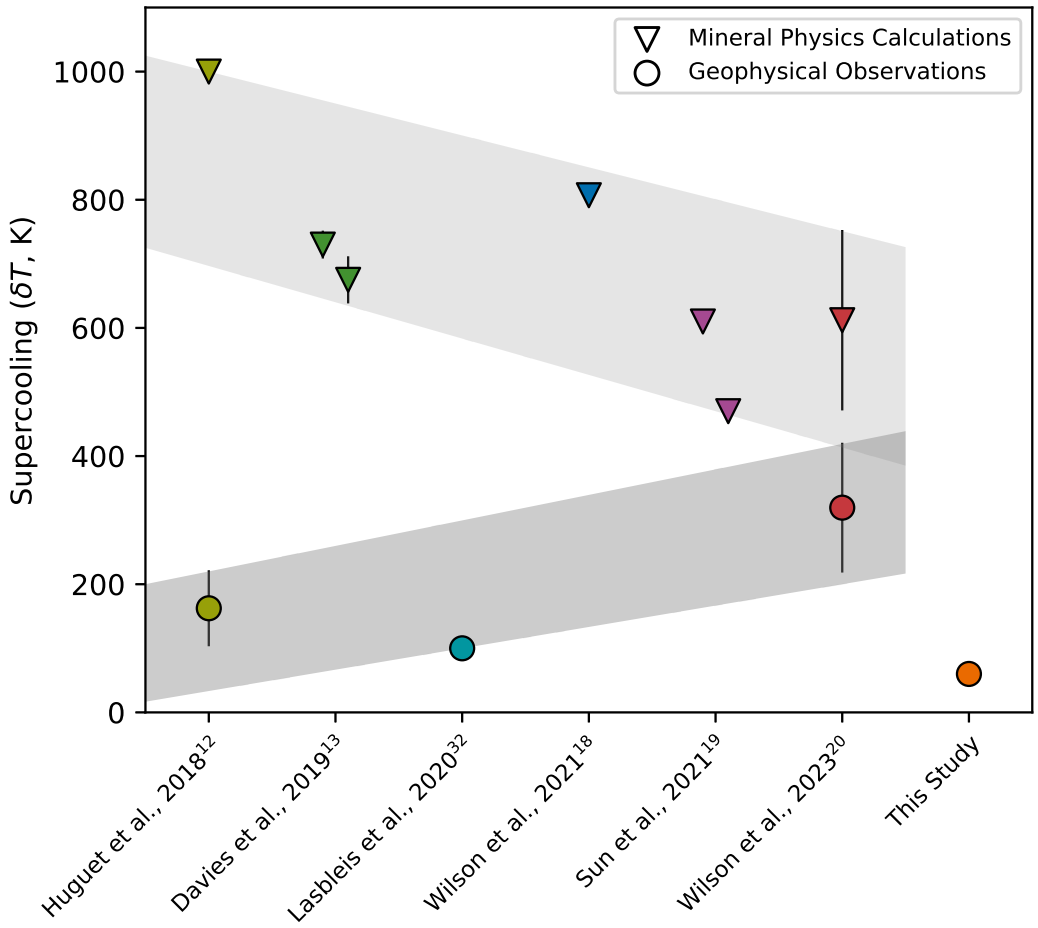

Figure 2. Published estimates of the supercooling in Earth's core. The supercooling required to nucleate the Earth's IC inferred from geophysical observations (circles, dark grey area; with a maximum of 419 K)[20] is compared estimated supercooling required to trigger nucleation of the IC according to studies applying mineral physics (squares, light grey area; with a minimum of 467 K[20]). Despite prior estimates of geophysically compatible and physically required supercooling converging (shaded areas), thermal history models from this study cannot reconcile supercooling greater than 60 K with constraints derived from the palaeomagnetic record and seismic observations (orange circle, see Section 4).

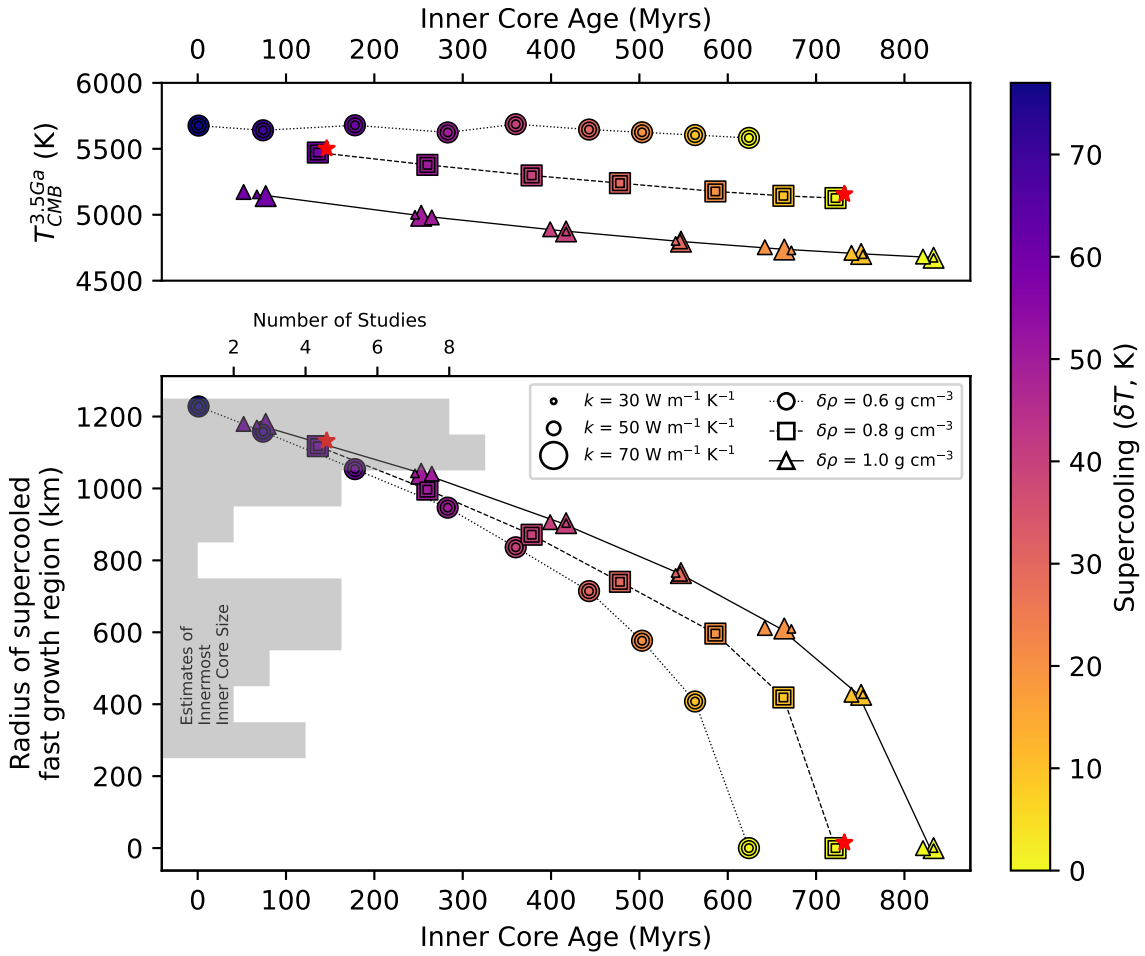

Figure 3. Outcomes of coupled core-mantle thermal histories with supercooling. Models which match constraints on present day IC radius and mantle temperature and heat flux as well as having sufficient entropy to drive the geodynamo for the past 3.5 Gyrs. Upper panel: Core mantle boundary temperature at 3.5 Ga and IC age. Lower panel: IC age and radius of the supercooled region prior to nucleation, which also corresponds to the fast growth region. Symbols are coloured according to the imposed supercooling δT. Three compositions which match estimates of density change across the inner core boundary[10] (circles, squares and triangles: $Fe_{0.82}O_{0.08}Si_{0.10}$, $Fe_{0.79}O_{0.13}Si_{0.08}$ and $Fe_{0.81}O_{0.17}Si_{0.02}$, respectively) and three thermal conductivities of the core (small, medium and large symbols: 30, 50 and 70 W m^{-1} K^{-1}) are explored. The supercooled region is assumed to be adiabatic (see section S4 of the Supplementary Information for isothermal cases). Cases shown in Fig. 6 are marked with red stars. A histogram (lower panel, grey) is presented showing the number of seismological studies which have identified radial changes in IC anisotropy (see Supplementary Information section S5 which collates these studies). Discussion of geophysical observations which relate to IC structure can be found in section 4. IC age is more sensitive to supercooling of the core prior to IC nucleation than composition or thermal conductivity and only cases with less than 80 K of supercooling are compatible with the observed size of the IC.

the assumed initial size of the supercooled region because the limiting factor is the drop in g as the region grows towards the equilibrium point where the temperature of the supercooled region intersects the melting temperature. In reality we would expect the latent heat to be removed by core convection; however, even this process is slow compared to the rapid growth of the supercooled region. Nevertheless we expect that convective heat transport would only increase the growth rate from that estimated above.

Light element partitioning offers another mechanism for slowing the freezing of supercooled liquids. Oxygen depresses the melting point of liquid iron, reducing δT for the same T, and is strongly partitioned to the liquid[25]. How light elements behave during rapid freezing is not obvious but if partitioned rapidly into the liquid ahead of the freezing interface, the growth rate of the IC might be controlled by the speed at which diffusion and advection can transport these light elements into the bulk core. However, once the growth rate becomes comparable to the timescale of outer core overturn (hundreds of years), fluid advection will presumably become efficient at mixing the chemical anomaly into the bulk core. Therefore the growth in the supercooled region is expected to be extremely fast compared to the equilibrium growth phase.

4 Implications of Supercooling for the Structure and Dynamics of the Inner core

It is a physical requirement that the liquid core was supercooled prior to IC nucleation. The exact value to which the constituent liquids were supercooled remains enigmatic however an upper limit of 100 K would be broadly consistent with inferences from geophysical observations (Figs 2 and 3). We now explore the consequences of supercooling for the structure and dynamics of the IC through time and how these might relate to seismic observations and the palaeomagnetic record.

4.1 Inner core structure

One of the key constraints on the thermal history of the deep Earth, the size of the IC, comes from seismology[65]. The transition between solid and liquid iron at 1221 km radius is assumed to define the intersection of T_m and T_a, fixing the present day thermal state of the core. The ICB is found to be sharp with a thickness of less than 3 km[66] although a laterally heterogeneous 4-8 km thick mushy layer between the inner and outer core might exist in some places[67]. The IC might grow through direct freezing but could also grow as a result of an iron snow which forms in the lowermost outer core[68]. If this snow regime is the relevant case, the thickness of the partially liquid region between the inner and outer core suggests that compaction of solids and expulsion of residual liquids upon late stages of core growth is efficient[32].

Seismic body waves and normal modes sampling the IC reveal both radial and lateral heterogeneity (see Fig. 4 and several review papers for a discussion[69,70]) but details of these features have been widely debated. Body waves are short period seismic data with a typical frequency of 0.1 to 1 Hz, which enables us to find small scale structures, including layers and discontinuities. Normal modes are whole Earth oscillations with frequencies varying from 1 to 10 mHz and therefore are only sensitive to large scale structures. Features which are seen with both body waves and normal modes are most robust, but it is also important to realise that some features could be challenging to be observed with normal modes.

Body waves show that the outermost 60-100 km of the IC consists of an isotropic layer where the eastern hemisphere transmits waves 1.5% faster than the western hemisphere[71,72]. This layer is also more strongly attenuating in the eastern hemisphere than in the western hemisphere[73]. Below this layer, the IC is found to be anisotropic with seismic body waves travelling parallel to the rotational axis of the Earth arriving several seconds earlier than those travelling parallel to the equatorial plane[74] and normal modes displaying anomalous zonal splitting[75]. Anisotropy is the most robust of all seismic features seen in the inner core, since it is found in both body waves and normal modes with the rotational direction being 2-3.5%[76,77] and 3-5%[78–84] faster for normal mode and body wave studies respectively. The anisotropy varies laterally where the western hemisphere appears to be more strongly anisotropic than the eastern hemisphere, which was initially only seen with body waves[85], but has also been confirmed by normal mode observations[86]. Attenuation anisotropy might also exist where waves travelling in the direction of the Earth's rotation axis see more amplitude reduction than equatorially oriented waves[87,88]. Anisotropy also varies radially and increases with depth. An innermost inner core (IMIC) has been proposed by several studies. This region represents a small sphere in the centre of the IC with a radius of 300-750 km and has a distinct anisotropy with a different slowest direction compared to the outermost part of the IC. The innermost inner core has been seen by a range of different seismic data types, including body waves[62,89,90] and normal modes[91] but also multiple reflected waves[92] and it is also a very clear feature in inner core tomographic models[63,83].

A histogram is shown in Fig. 3 presenting the number of studies which find a radial change in isotropic and anisotropic structure, both elastic and attenuating, at any depth in the IC. There are roughly two depth ranges in which the anisotropy changes markedly, which have been confirmed by a large number of studies. Near the top, there is a change around 1100-1200km radius which signifies the change from isotropic to anisotropic structure. Then at a range of 300 to 750 km radius there is the change to the inner most inner core. Here we will focus primarily on mechanisms which explain the variation of elastic anisotropy with radius, starting with the traditional view, where the core was never supercooled.

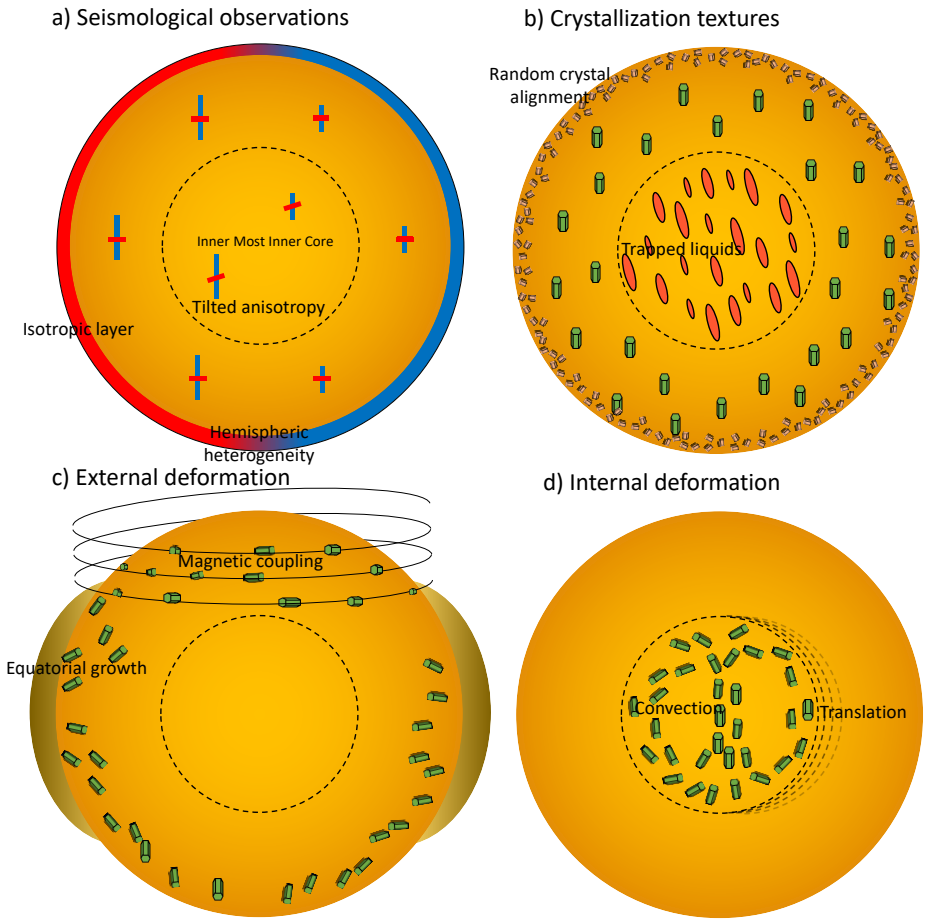

Figure 4. Observation and emplacement of IC structure. a) Radial and lateral heterogeneity in the velocity and anisotropy of Earth's core. These features must result from compositional or textural heterogeneities which have multiple potential origins. b) Freezing of liquid iron alloys can produce different grain sizes and orientations as well as the trapping of liquids. c) External forces such as the magnetic coupling and relaxation of equatorial growth might orient crystals in the IC during or after their crystallisation. d) Internal deformation mechanisms arising from IC convection could establish stress regimes which reorient IC crystals. The structure of the IC inferred from seismology has several might have its origin in several mechanisms for developing texture, some of which are unique to a supercooled core. **Note for reviewers: Illustrations will be reproduced by the editorial artist if accepted.**

4.2 Inner core dynamics

Several mechanisms have been proposed to generate the observed elastic anisotropy (Fig 4). Solidification texturing could align crystals during the freezing process[93,94], while deformation aligns the crystals after solidification and produces texture through accumulated strain. Several different deformation texturing mechanisms have been proposed. Internally-induced deformation texturing can arise if the IC is unstable to thermal or chemical convection[95]. Externally-induced deformation texturing can arise via topographic relaxation of the ICB driven by latitudinal variations in IC growth associated with outer core convection[96], flow induced by coupling to the magnetic field[97,98], or flow driven by differential heat flux arising from outer core convection[90]. The dominant mechanism depends on the IC growth history and material properties[99] and could have varied over time.

If the IC is convectively unstable then the strain produced by the resultant flow is expected to dominate over other deformation mechanisms[99]. The conditions for instability rely on some poorly known quantities, particularly the IC growth rate and thermal and chemical diffusivities. Nevertheless, for plausible growth histories that ignore supercooling there is a consensus that convection becomes less likely as the IC grows and its growth rate declines[100–102]. For low values of the thermal conductivity (~ 30 W m^{-1} K^{-1}) an early episode of thermal convection is possible[101,103], while for the high conductivity values > 100 W m^{-1} K^{-1} obtained by mineral physics calculations at ICB conditions[104,105] it is very likely that thermal convection has never occurred. Compositional convection can be driven by a change in light element partitioning with depth[106] (and hence time); however, current models suggest that this destabilising effect only dominates when the IC is less than about half its present size[11]. Another possibility is that convection can result from imposed lateral heat flux variations at the ICB[90], perhaps deriving from thermal interactions between the lower mantle and liquid core[107], though whether rapidly rotating convection can transmit such variations to the ICB is currently debated[108].

In the early period where convection was possible, two distinct flow regimes have been identified that depend primarily on the IC viscosity[99,103] η. For $\eta \lesssim 10^{18}$ Pa s plume convection dominates and becomes increasingly chaotic as the Rayleigh number increases, while for higher η a spherical harmonic degree 1 translation emerges that can lead to melting of the IC if the translation velocity is fast enough. A double diffusive form of the translation can arise even if the destabilising compositional gradient is much weaker than the stabilising thermal gradient, though this mode requires a higher viscosity and has a weaker velocity that pure thermal translation[109]. The resulting accumulated strain is probably weak for plume convection[110], because the flow is strongly time-dependent[99], and also the double diffusive translation, because the growth rate of the instability is on the order of the IC age[109]. For thermal translation the strain rates can be appreciable as long as the viscosity is not too high. This flow is a good candidate for generating hemispheric asymmetry[111,112]. Though the strain field does not display the alignment with the rotation axis required to explain the cylindrical anisotropy.

For convectively stabilising conditions the primary strain-producing mechanisms are thought to be due to topographic relaxation and magnetic coupling[99]. Topographic relaxation arises from the assumption (supported by numerical simulations[107]) that core convection enhances ICB heat flow (and hence solidification rate) in the equatorial region, with isostatic adjustment driving a spherical harmonic degree 2 flow from the equatorial region towards the poles[96]. If the IC is neutrally stratified then the resulting flow penetrates deep into the IC and can explain the general increase of anisotropy with depth[90,113] . However, with increasing stratification the flow becomes confined to a thin layer below the ICB with negligible deformation at depth[100,113] unless the viscosity is very high ($\sim 10^{23}$ Pa s[99]), in which case the strain rates decline substantially. The flow induced through coupling to the azimuthal component of the Lorentz force is unaffected by stratification[114] and yields an accumulated strain that is maximum at mid-depth[115]. However, the mechanism relies on a low viscosity of $\eta \lesssim 10^{12}$ Pa s in order for the strain rate to exceed that from topographic relaxation of equatorial growth, and an assumed configuration of the magnetic field at the ICB now and back in time, which is not directly observable.

In summary, in the absence of supercooling the IC appears to have been stably stratified throughout most of its history, suggesting that convection is not the primary cause of radial anisotropy variations. The most likely deformation texturing mechanisms are magnetic coupling through the azimuthal Lorentz force, which requires a low viscosity, or topographic coupling, which requires a high viscosity and a timescale for texture development on the order of the IC age. Hemispherical growth could also produce the outer isoptropic layer if the stratification is strong enough[100]. These mechanisms could be augmented by other processes such as translational flow induced by lateral heat flow variations at the ICB, which might be important for explaining the hemispheric asymmetry. We now discuss how this picture changes with the addition of supercooling. The key difference is the period of rapid growth (Section 3) following nucleation, which alters the dynamical processes that can cause deformation in the deep IC.

Following nucleation the IC growth rate is estimated to be far in excess of ~ 1 mm yr^{-1} (Section 3). This growth rate yields a Rayleigh number that far exceeds the critical value for instability for any value of the viscosity[103]. The critical values published to date[103] have ignored the time-dependence of the basic diffusive state, which could be important in the rapid growth regime. Nevertheless, the available values indicate that the IC was initially inevitably unstable to both plume and translation modes of convection. However, the supercooled region would have frozen in perhaps only a century, after which the Rayleigh number likely fell below the critical value for convection. A detailed study of the flow instability in this scenario would require

modelling the coupled dynamics of inner and outer core since the two systems evolve on similar timescales. However, present estimates of the growth rate for both plume and translation flows, which again neglect the rapid change of the basic state, are estimated to be a few tens of millions of years[103], suggesting that the instability would not develop despite the strongly unstable conditions.

Texturing of the supercooled material could arise either from solidification texturing, magnetic coupling (penetrating the rapidly frozen region), or equatorial growth. Magnetic coupling during fast freezing might be relatively unaffected by rapid cooling if the abrupt changes in geometry and thermo-chemical buoyancy have a relatively short-term impact on the dynamo. For equatorial growth a key factor is the length of time required to establish the stratified thermal and chemical profiles from the temperature and composition at which the material froze (presumably between the adiabatic well-mixed pre-nucleation state and the liquidus). If this timescale is short then the initial flow induced by topographic relaxation would be confined to the edge of the supercooled region; otherwise the flow can penetrate to the centre of the core.

Rapid crystal growth might trap liquids within the IC. The shape of liquid inclusions and mineralogy resulting from their eventual freezing could influence the attenuation and velocity anisotropy of this region. Partitioning of light elements to the liquid can depress the melting temperature of these trapped liquids, delaying freezing. The degree to which this effect is preserved to the present day depends strongly on the compaction efficiency of the newly formed crystal matrix[32] and partitioning behaviour during quenching, neither of which are well understood at core conditions. Due to light element partitioning, these inclusions would freeze slowly as the IC cooled and 3-10 %[21] of the IC could remain at the present day, providing a plausible explanation for anomalously slow S-wave speeds[116] in the bulk IC when compared to mineral physics[117,118]. Lasbleis et al.[32] suggested the slower freezing rate of trapped liquids could imprint a heterogeneous texture in the innermost IC and explain why its anisotropy is different compared to the shallower parts of the IC. One mechanism for this structure is for the crystals freezing in these liquid inclusions to experience magnetic coupling. Ab initio calculations[119,120] have shown that the principle axis of magnetic susceptibility in HCP Fe is orthogonal to the axis of elastic anisotropy. If magnetically coupled, crystals would have an elastic anisotropic alignment parallel to the rotation axis of the core. The field strength needed to align the crystal structure in the solid is likely very strong[120] but if crystals grow within liquid inclusions, exposed to the magnetic field but isolated from convection, texturing is more plausible. Similarly, crystal growth within liquid inclusions could be enhanced along principal heat flux directions[93] producing a textural alignment flowing from the equator to the poles[96].

4.3 Palaeomagnetic evidence of inner core growth

The introduction of supercooling opens the possibility that a rapidly frozen region accounts for some or all of the radial heterogeneity in the IC (Fig. 5). IC translation appears to still be required to explain lateral heterogeneity but supercooling might help with initiation. Because nucleation can occur anywhere with the supercooled volume fast freezing could begin away from the centre of the Earth, this offset might initiate translational growth or offset texturing. Convection in the supercooled region appears unlikely despite the strongly unstable conditions because the timescale for instability is much longer than the freezing timescale. The viability of texture development by magnetic coupling or heterogeneous growth is less clear than in the classical case with no undercooling as it depends on the uncertain properties of the growth process. Solidification textures resulting from rapid freezing of the supercooled region and liquid inclusions captured in the process are likely to be distinct from those associated with slower growth. A more detailed model of freezing and partitioning under supercooled conditions at high temperature and pressure is required to understand the potential for generating anisotropic texture in the IC. Additionally, an improved understanding of geodynamo activity during and following a rapid freezing event is needed to qualify magnetic coupling.

The palaeomagnetic record captures long-term changes in the strength of the magnetic field. Nucleation of the IC might have an observable signature in the record in a number of ways. Theoretical models without supercooling[121,122] suggest that over time the dynamo power and hence the dipole moment (DM) decline to a weak state directly preceding IC formation, after which latent heat and gravitational energy release from IC growth provide substantial excess power to the geodynamo, causing a sudden increase in field strength (Fig. 6). An ultra-low DM followed by a rapid increase has been reported in the early Cambrian[15,123,124] and weak fields have also been reported in the neo-proterozoic[125], though some high intensities around 1.1 Ga appear inconsistent with the simple theoretical prediction[126]. The addition of supercooling changes the theoretical prediction in two ways. First, increasing δT decreases the theoretical IC age (Fig. 3) and increases the predicted rate of DM intensification at the formation of the IC (Fig. 6). This information will hopefully enable future paleomagnetic analyses to constrain the minimum age of the IC that is compatible with the paleointensity record, which should improve existing bounds on the viable supercooling (Fig. 2). Second, rapid growth of the supercooled region and the associated release of latent heat and gravitational energy from chemical partitioning (which is not included in the models in Fig.6) should drastically increase the power available to the dynamo, which could have left an imprint on the paleomagnetic record[12]. Power-based scaling laws[121,122] derived from simulations of the dynamo in the past 100 Myrs would predict a dramatic increase in the surface dipole field strength during this period, which could far exceed that shown by the purple line in Fig. 6. However, simulations also show

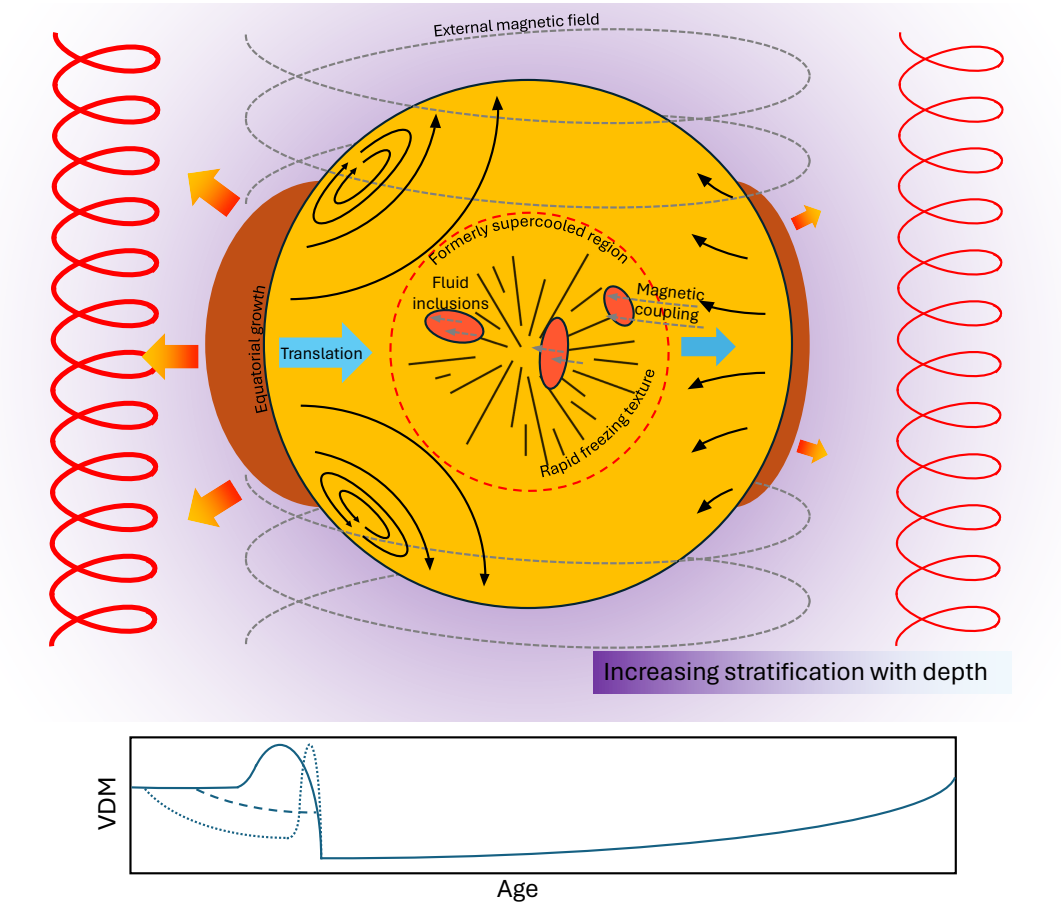

Figure 5. Multiple mechanisms for producing IC heterogeneity. Without supercooling, equatorial growth, thermal and chemical convection, translational growth and the magnetic coupling all offer routes to generate heterogeneous texture in the IC. With supercooling some of these are modified or apply to different regions of the IC and the rapid growth of the IC introduces the potential for unique texturing from solidification and trapped liquids. Multiple mechanisms for developing texture in the IC might be needed to explain all seismologically detected structure. **Note for reviewers: Illustrations will be reproduced by the editorial artist if accepted.**

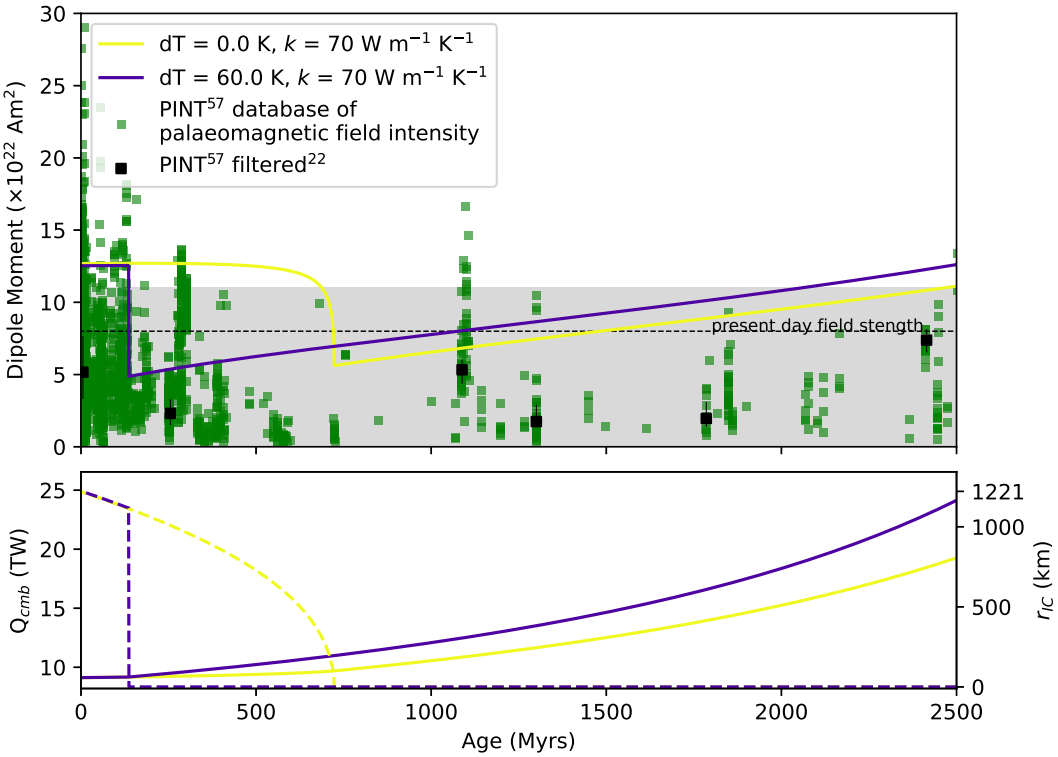

Figure 6. Comparing thermal history models with the palaeomagnetic record. Upper: Dipole moment calculated from two thermal history cases (red stars Fig. 3), with (blue) and without (yellow) supercooling prior to nucleation. Palaeomagnetic intensity data (green squares: PINT[57], black squares: filtered PINT dataset from Davies et al.[122]) and the present-day field strength (black dashed line) are shown for reference . Lower: CMB heat flow (solid lines) is shown for the same cases in the upper panel along side the IC radius with time (dashed lines). Models with supercooling greater than 40 K produce a core less than 300 Myrs old, which is challenging to reconcile with the palaeomagnetic record which shows consistently high field strength during this period.

that increased thermo-chemical driving eventually leads to a loss of axial dipole dominance and a weak multipolar field[127,128]. Therefore the rapid increase in field strength could be curtailed by dipole collapse, followed by a period of weak highly variable field behaviour. Future dynamo simulations and paleomagnetic analyses will hopefully shed more light on this issue.

5 Summary and Future Perspectives

Supercooling is required for freezing of Earth's solid IC to have begun, as with any liquid. The degree to which the liquid core was supercooled prior to nucleation remains enigmatic but is crucial to understanding of the Earth's deep interior. Nucleation of the IC was perhaps the most significant event in the thermal history of the deep Earth and brought about the current thermal state of the core. Molecular dynamic simulations of liquid iron alloys at the conditions of Earth's core suggest that several hundred degrees of supercooling is required for spontaneous freezing. Here we have shown that a supercooling of 100 K is broadly compatible with palaeomagnetic and geophysical constraints.

To complete the picture of IC nucleation a viable resolution to the inner core nucleation paradox is needed. Through solving the paradox, an acceptable value of supercooling in the core will be realised and thermal history models can become consistent with both mineral physics and observations. A resolution to the inner core nucleation paradox requires new mineral physics calculations which explore more complex compositions in the core than previous studies. The simple binary compositions tested thus far have revealed that homogeneous nucleation might be possible in the core but have fallen short of a definitive resolution, especially given the small value of supercooling compatible with geophysical and palaeomagnetic constraints found in the models presented here. Additionally, a more detailed understanding of interfacial energy of nucleating solids in the Earth's core is needed, where existing estimates are sparse, requiring specific attention from computational mineral physics. Heterogeneous nucleation should be explored as well because this also offers a viable mechanism for nucleating the inner core. At the time of writing, no pre-existing solid surfaces have been identified to act as heterogeneous nucleation sites in the core.

Research into potential solid phases which might avoid dissolution and melting in the core is needed to identify a resolution to the paradox via heterogeneous nucleation.

Once defined, a resolution to the nucleation paradox will specify the amount by which the core was supercooled prior to nucleation. Calculations of alloy freezing rates suggest that inner core growth following the nucleation event was extremely fast but crystal growth behaviour under core conditions at these rates is not understood. Both experimental and computational research is needed to better understand freezing textures, element partitioning and residual liquid entrapment at scales ranging from angstroms to meters. This research will facilitate more nuanced predictions of inner core growth rate as well as the textural, structural and thermo-chemical fingerprints of inner core nucleation which might be identified through palaeomagnetic and seismological investigation.

A detailed picture of how the inner core first nucleated will emerge as a result of a resolution to the paradox and description of rapid freezing in the supercooled liquid core. However, the present view of inner and outer core dynamics typically assumes that processes evolve on a timescale of at least 10,000 years, rendering both inapplicable to the time immediately after nucleation. New dynamo calculations and scaling laws are needed to describe outer core dynamics when the inner and outer cores evolve on comparable timescales, as could be the case during the rapid growth phase of the inner core. These advances are essential for understanding how inner core nucleation has impacted the dynamics of the inner core, especially with regards to the palaeomagnetic record and convective instabilities in the growing inner core.

Finally, a model which explains all seismically inferred inner core structure does not yet exist. This review has highlighted that of the existing mechanisms to develop crystallographic texture in the solid inner core, some are unique to a supercooled liquid core, some are modified by this supercooled scenario and other mechanisms are independent of it. The models presented here might explain two seismically distinct regions of the inner core resulting from rapid freezing and subsequent slower growth but do not explain lateral heterogeneity or the presence of more than two layers. Because many of the proposed mechanisms for generating inner core texture do not influence the entire inner core but are capable of overprinting the signatures of older processes it is not obvious which combination mechanisms is capable of matching seismological data. To address this issue, a holistic model of the inner core thermal history is needed. This model might include descriptions of freezing, dynamics and crystallographic deformation and seek to explain the complex history of Earth's solid inner core.

Acknowledgements

We acknowledge a Natural Environment Research Council grant, reference NE/T000228/1, which supports AJW, AMW, DA, MP and CD authors on this project. AJW and CD acknowledge support from the Natural Environment Research Council (NERC) grant number NE/V010867/1. AMW and CD acknowledge support from the Natural Environment Research Council (NERC) grant number NE/T004835/1. DA and MP acknowledge support from the Natural Environment Research Council (NERC) grant numbers NE/M000990/1 and NE/R000425/1. AD acknowledges support from European Research Council (ERC) under the European Union's Horizon 2020 research and innovation programme (grant agreement No. 681535 - ATUNE) and a Vici award number 016.160.310/526 from the Netherlands Organisation for Scientific Research (NWO). We thank Marine Lasbleis for her helpful discussion on the dynamics of the inner core. For the purpose of open access, the authors have applied a CC BY pubic copyright license to any Author Accepted Manuscript version arising.

Author contributions

All authors contributed to **conceptualization** of this review and the **review and editing** process of writing the manuscript. AD carried out data curation for all seismological evidence used. AJW, AMW and CD developed the **methodologies**, thermal history models and other analytical approaches, used to synthesise previous studies and carried out the **investigation**. AMW, CD and DA acquired funding which supported this project. AJW conducted the **formal analysis** and **writing of the original draft**.

Competing interests

The authors have no competing interests to declare.

References

1. Braginsky, S. Structure of the f layer and reasons for convection in the earth's core. In *Soviet Phys. Dokl.*, vol. 149, 8–10 (1963).

2. Nimmo, F. Energetics of the core. In Schubert, G. (ed.) *Treatise on geophysics 2nd Edn*, vol. 8, 27–55 (Elsevier, Amsterdam, 2015).

3. Stevenson, D. J. Mars' core and magnetism. *Nature* **412**, 214–219 (2001).

4. Wilson, A. J. *et al.* Powering earth's ancient dynamo with silicon precipitation. *Geophys. Res. Lett.* **49**, e2022GL100692 (2022).

5. O'Rourke, J. G. & Stevenson, D. J. Powering Earth's dynamo with magnesium precipitation from the core. *Nature* **529**, 387–389 (2016).

6. Badro, J. *et al.* Magnesium partitioning between Earth's mantle and core and its potential to drive an early exsolution geodynamo. *Geophys. Res. Lett.* **45**, 13–240 (2018).

7. Hirose, K. *et al.* Crystallization of silicon dioxide and compositional evolution of the Earth's core. *Nature* **543**, 99–102 (2017).

8. Nimmo, F., Price, G., Brodholt, J. & Gubbins, D. The influence of potassium on core and geodynamo evolution. *Geophys. J. Int.* **156**, 363–376 (2004).

9. Wilson, A. J., Pozzo, M., Davies, C. J., Walker, A. M. & Alfè, D. Examining the power supplied to earth's dynamo by magnesium precipitation and radiogenic heat production. *Phys. Earth Planet. Interiors* **343**, 107073 (2023).

10. Davies, C., Pozzo, M., Gubbins, D. & Alfè, D. Constraints from material properties on the dynamics and evolution of Earth's core. *Nat. Geosci.* **8**, 678–685 (2015).

11. Labrosse, S. Thermal evolution of the core with a high thermal conductivity. *Phys. Earth Planet. Interiors* **247**, 36–55 (2015).

12. Huguet, L., Van Orman, J. A., Hauck II, S. A. & Willard, M. A. Earth's inner core nucleation paradox. *Earth Planet. Sci. Lett.* **487**, 9–20 (2018).

13. Davies, C., Pozzo, M. & Alfè, D. Assessing the inner core nucleation paradox with atomic-scale simulations. *Earth Planet. Sci. Lett.* **507**, 1–9 (2019).

14. Tarduno, J. A. *et al.* Geodynamo, solar wind, and magnetopause 3.4 to 3.45 billion years ago. *science* **327**, 1238–1240 (2010).

15. Bono, R. K., Tarduno, J. A., Nimmo, F. & Cottrell, R. D. Young inner core inferred from ediacaran ultra-low geomagnetic field intensity. *Nat. Geosci.* **12**, 143–147 (2019).

16. Tabazadeh, A., Djikaev, Y. S. & Reiss, H. Surface crystallization of supercooled water in clouds. *Proc. Natl. Acad. Sci.* **99**, 15873–15878 (2002).

17. Christian, J. W. *The theory of transformations in metals and alloys* (Newnes, 2002).

18. Wilson, A. J., Walker, A. M., Alfè, D. & Davies, C. J. Probing the nucleation of iron in earth's core using molecular dynamics simulations of supercooled liquids. *Phys. Rev. B* **103**, 214113 (2021).

19. Sun, Y., Zhang, F., Mendelev, M. I., Wentzcovitch, R. M. & Ho, K.-M. Two-step nucleation of the earth's inner core. *Proc. Natl. Acad. Sci.* **119**, e2113059119 (2022).

20. Wilson, A. J., Alfè, D., Walker, A. M. & Davies, C. J. Can homogeneous nucleation resolve the inner core nucleation paradox? *Earth Planet. Sci. Lett.* **614**, 118176 (2023).

21. Singh, S., Taylor, M. & Montagner, J. On the presence of liquid in earth's inner core. *Science* **287**, 2471–2474 (2000).

22. Pang, G. *et al.* Enhanced inner core fine-scale heterogeneity towards earth's centre. *Nature* **620**, 570–575 (2023).

23. Alfè, D., Gillan, M. & Price, G. D. Composition and temperature of the Earth's core constrained by combining ab initio calculations and seismic data. *Earth Planet. Sci. Lett.* **195**, 91–98 (2002).

24. Li, Y., Vočadlo, L., Alfè, D. & Brodholt, J. Carbon partitioning between the Earth's inner and outer core. *J. Geophys. Res. Solid Earth* **124**, 12812–12824 (2019).

25. Alfè, D., Gillan, M. & Price, G. Temperature and composition of the Earth's core. *Contemp. Phys.* **48**, 63–80 (2007).

26. Wood, B. J., Li, J. & Shahar, A. Carbon in the core: its influence on the properties of core and mantle. *Rev. Mineral. Geochem.* **75**, 231–250 (2013).

27. Blanchard, I. *et al.* The metal–silicate partitioning of carbon during earth's accretion and its distribution in the early solar system. *Earth Planet. Sci. Lett.* **580**, 117374 (2022).

28. Smith, E. M. *et al.* Large gem diamonds from metallic liquid in earth's deep mantle. *Science* **354**, 1403–1405 (2016).

29. Fischer, R. A., Campbell, A. J. & Ciesla, F. J. Sensitivities of Earth's core and mantle compositions to accretion and differentiation processes. *Earth Planet. Sci. Lett.* **458**, 252–262 (2017).

30. Badro, J., Siebert, J. & Nimmo, F. An early geodynamo driven by exsolution of mantle components from Earth's core. *Nature* **536**, 326–328 (2016).

31. Eustathopoulos, N. Wetting by liquid metals—application in materials processing: the contribution of the grenoble group. *Metals* **5**, 350–370 (2015).

32. Lasbleis, M., Kervazo, M. & Choblet, G. The fate of liquids trapped during the earth's inner core growth. *Geophys. Res. Lett.* **47**, e2019GL085654 (2020).

33. Spaepen, F. & Turnbull, D. Kinetics of motion of crystal-melt interfaces. In Grant, N. J. & Giessen, B. C. (eds.) *Rapidly Quenched Metals*, 205 (M.I.T. Press, Cambridge, Ma, 1976).

34. Sun, G., Xu, J. & Harrowell, P. The mechanism of the ultrafast crystal growth of pure metals from their melts. *Nat. materials* **17**, 881–886 (2018).

35. Coriell, S. & Turnbull, D. Relative roles of heat transport and interface rearrangement rates in the rapid growth of crystals in undercooled melts. *Acta Metall.* **30**, 2135–2139 (1982).

36. Davies, C. Cooling history of earth's core with high thermal conductivity. *Phys. Earth Planet. Interiors* **247**, 65–79 (2015).

37. Greenwood, S., Davies, C. J. & Mound, J. E. On the evolution of thermally stratified layers at the top of Earth's core. *Phys. Earth Planet. Interiors* 106763 (2021).

38. Driscoll, P. & Davies, C. The "new core paradox:" challenges and potential solutions. *J. Geophys. Res. Solid Earth* e2022JB025355 (2023).

39. Driscoll, P. & Bercovici, D. On the thermal and magnetic histories of Earth and Venus: Influences of melting, radioactivity, and conductivity. *Phys. Earth Planet. Interiors* **236**, 36–51 (2014).

40. Buffett, B. A. & Seagle, C. T. Stratification of the top of the core due to chemical interactions with the mantle. *J. Geophys. Res. Solid Earth* **115** (2010).

41. Labrosse, S., Hernlund, J. & Coltice, N. A crystallizing dense magma ocean at the base of the earth's mantle. *Nature* **450**, 866–869 (2007).

42. Davies, C. & Greenwood, S. Thermo-chemical dynamics in Earth's core arising from interactions with the mantle. *eartharxiv.org* **0**, 0 (2022).

43. O'Rourke, J. G., Korenaga, J. & Stevenson, D. J. Thermal evolution of earth with magnesium precipitation in the core. *Earth Planet. Sci. Lett.* **458**, 263–272 (2017).

44. Al Asad, M., Lau, H. C., Crowley, J. W. & Lenardic, A. Modes of mantle convection, their stability, and what controls their existence. *J. Geophys. Res. Solid Earth* **128**, e2023JB027274 (2023).

45. Masters, G. & Gubbins, D. On the resolution of density within the earth. *Phys. Earth Planet. Interiors* **140**, 159–167 (2003).

46. Alfè, D., Price, G. & Gillan, M. Iron under Earth's core conditions: Liquid-state thermodynamics and high-pressure melting curve from ab initio calculations. *Phys. Rev. B* **65**, 165118 (2002).

47. Sinmyo, R., Hirose, K. & Ohishi, Y. Melting curve of iron to 290 gpa determined in a resistance-heated diamond-anvil cell. *Earth Planet. Sci. Lett.* **510**, 45–52 (2019).

48. Li, J. *et al.* Shock melting curve of iron: A consensus on the temperature at the earth's inner core boundary. *Geophys. Res. Lett.* **47**, e2020GL087758 (2020).

49. Gomi, H. *et al.* The high conductivity of iron and thermal evolution of the Earth's core. *Phys. Earth Planet. Interiors* **224**, 88–103 (2013).

50. Pozzo, M., Davies, C., Gubbins, D. & Alfè, D. Thermal and electrical conductivity of iron at Earth's core conditions. *Nature* **485**, 355–358 (2012).

51. Konôpková, Z., McWilliams, R. S., Gomez-Perez, N. & Goncharov, A. F. Direct measurement of thermal conductivity in solid iron at planetary core conditions. *Nature* **534**, 99–101 (2016).

52. Zhang, Y. *et al.* Reconciliation of experiments and theory on transport properties of iron and the geodynamo. *Phys. review letters* **125**, 078501 (2020).

53. Biggin, A. J. *et al.* Palaeomagnetic field intensity variations suggest mesoproterozoic inner-core nucleation. *Nature* **526**, 245–248 (2015).

54. Tarduno, J. A., Cottrell, R. D., Davis, W. J., Nimmo, F. & Bono, R. K. A hadean to paleoarchean geodynamo recorded by single zircon crystals. *Science* **349**, 521–524 (2015).

55. Tarduno, J. A. *et al.* Paleomagnetism indicates that primary magnetite in zircon records a strong hadean geodynamo. *Proc. Natl. Acad. Sci.* **117**, 2309–2318 (2020).

56. Fu, R. R. *et al.* Paleomagnetism of 3.5-4.0 ga zircons from the barberton greenstone belt, south africa. *Earth Planet. Sci. Lett.* **567**, 116999 (2021).

57. Bono, R. K. *et al.* The pint database: a definitive compilation of absolute palaeomagnetic intensity determinations since 4 billion years ago. *Geophys. J. Int.* **229**, 522–545 (2022).

58. Katsura, T., Yoneda, A., Yamazaki, D., Yoshino, T. & Ito, E. Adiabatic temperature profile in the mantle. *Phys. Earth Planet. Interiors* **183**, 212–218 (2010).

59. Jaupart, C., Labrosse, S., Lucazeau, F. & Mareschal, J. 7.06-temperatures, heat and energy in the mantle of the earth. *Treatise on geophysics* **7**, 223–270 (2007).

60. Andrault, D. *et al.* Solidus and liquidus profiles of chondritic mantle: Implication for melting of the earth across its history. *Earth planetary science letters* **304**, 251–259 (2011).

61. Nimmo, F. Thermal and compositional evolution of the core. *Treatise on Geophys.* **9**, 201–219 (2015).

62. Ishii, M. & Dziewoński, A. M. The innermost inner core of the earth: Evidence for a change in anisotropic behavior at the radius of about 300 km. *Proc. Natl. Acad. Sci.* **99**, 14026–14030 (2002).

63. Brett, H., Hawkins, R., Waszek, L., Lythgoe, K. & Deuss, A. 3d transdimensional seismic tomography of the inner core. *Earth Planet. Sci. Lett.* **593**, 117688 (2022).

64. Komabayashi, T. Thermodynamics of the system Fe–Si–O under high pressure and temperature and its implications for Earth's core. *Phys. Chem. Miner.* **47**, 1–13 (2020).

65. Dziewonski, A. M. & Anderson, D. L. Preliminary reference earth model. *Phys. earth planetary interiors* **25**, 297–356 (1981).

66. Koper, K. D., Pyle, M. L. & Franks, J. M. Constraints on aspherical core structure from pkikp-pcp differential travel times. *J. Geophys. Res. Solid Earth* **108** (2003).

67. Tian, D. & Wen, L. Seismological evidence for a localized mushy zone at the earth's inner core boundary. *Nat. communications* **8**, 165 (2017).

68. Wong, J., Davies, C. J. & Jones, C. A. A regime diagram for the slurry f-layer at the base of earth's outer core. *Earth Planet. Sci. Lett.* **560**, 116791 (2021).

69. Deuss, A. Heterogeneity and anisotropy of earth's inner core. *Annu. Rev. Earth Planet. Sci.* **42**, 103–126 (2014).

70. Tkalcic, H. *The Earth's Inner Core Revealed by Observational Seismology* (Cambridge University Press, 2017).

71. Niu, F. & Wen, L. Hemispherical variations in seismic velocity at the top of the Earth's inner core. *Nature* **410**, 1081–1084 (2001).

72. Waszek, L. & Deuss, A. Distinct layering in the hemispherical seismic velocity structure of earth's upper inner core. *J. Geophys. Res. Solid Earth* **116** (2011).

73. Yu, W. & Wen, L. Seismic velocity and attenuation structures in the top 400 km of the Earth's inner core along equatorial paths. *J. Geophys. Res.* **112**, B07308 (2006).

74. Morelli, A., Dziewonski, A. M. & Woodhouse, J. H. Anisotropy of the inner core inferred from PKIKP travel times. *Geophys. Res Lett* **13**, 1545–1548 (1986).

75. Woodhouse, J. H., Giardini, D. & Li, X. D. Evidence for inner core anisotropy from free oscillations. *Geophys. Res Lett* **13**, 1549–1552 (1986).

76. Tromp, J. Support for anisotropy of the Earth's inner core from free oscillations. *Nature* **366**, 678–681 (1993).

77. Deuss, A., Ritsema, J. & van Heijst, H. A new catalogue of normal-mode splitting function measurements up to 10 mhz. *Geophys. J. Int.* **193**, 920–937 (2013).

78. Creager, K. C. Anisotropy of the inner core from differential travel times of the phases pkp and pkikp. *Nature* **356**, 309–314 (1992).

79. Vinnik, L., Romanowicz, B. & Breger, L. Anisotropy in the center of the inner core. *Geophys. research letters* **21**, 1671–1674 (1994).

80. McSweeney, T. J., Creager, K. C. & Merrill, R. T. Depth extent of inner-core seismic anisotropy and implications for geomagnetism. *Phys. earth planetary interiors* **101**, 131–156 (1997).

81. Creager, K. C. Large-scale variations in inner core anisotropy. *J. Geophys. Res. Solid Earth* **104**, 23127–23139 (1999).

82. Garcia, R. & Souriau, A. Inner core anisotropy and heterogeneity level. *Geophys. research letters* **27**, 3121–3124 (2000).

83. Sun, X. & Song, X. Tomographic inversion for three-dimensional anisotropy of earth's inner core. *Phys. Earth Planet. Interiors* **167**, 53–70 (2008).

84. Irving, J. C. E. & Deuss, A. Hemispherical structure in inner core velocity anisotropy. *J. Geophys. Res. Solid Earth* **116** (2011).

85. Tanaka, S. & Hamaguchi, H. Degree one heterogeneity and hemispherical variation of anisotropy in the inner core from PKP(BC)-PKP(DF) times. *J Geophys. Res* **102**, 2925–2938 (1997).

86. Deuss, A., Irving, J. C. E. & Woodhouse, J. H. Regional variation of inner core anisotropy from seismic normal mode observations. *Science* **328**, 1018–1020 (2010).

87. Souriau, A. & Romanowicz, B. Anisotropy in inner core attenuation: A new type of data to constrain the nature of the solid core. *Geophys. Res Lett* **23**, 1–4 (1996).

88. Makinen, A. M. & Deuss, A. Normal mode splitting due to inner core attenuation anisotropy. *Geophys. J. Int.* **195**, 1786–1795 (2013).

89. Wang, T., Song, X. & Xia, H. H. Equatorial anisotropy in the inner part of earth's inner core from autocorrelation of earthquake coda. *Nat. Geosci.* **8**, 224–227 (2015).

90. Frost, D. A., Lasbleis, M., Chandler, B. & Romanowicz, B. Dynamic history of the inner core constrained by seismic anisotropy. *Nat. Geosci.* **14**, 531–535 (2021).

91. Beghein, C. & Trampert, J. Robust normal mode constraints on inner-core anisotropy from model space search. *Science* **299**, 552–555 (2003).

92. Phạm, T.-S. & Tkalčić, H. Up-to-fivefold reverberating waves through the earth's center and distinctly anisotropic innermost inner core. *Nat. Commun.* **14**, 754 (2023).

93. Bergman, M. I. Measurements of electric anisotropy due to solidification texturing and the implications for the earth's inner core. *Nature* **389**, 60–63 (1997).

94. Bergman, M. I., Agrawal, S., Carter, M. & Macleod-Silberstein, M. Transverse solidification textures in hexagonal close-packed alloys. *J. crystal growth* **255**, 204–211 (2003).

95. Cottaar, S. & Buffett, B. Convection in the earth's inner core. *Phys. Earth Planet. Interiors* **198**, 67–78 (2012).

96. Yoshida, S., Sumita, I. & Kumazawa, M. Growth model of the inner core coupled with the outer core dynamics and the resulting elastic anisotropy. *J. Geophys. Res. Solid Earth* **101**, 28085–28103 (1996).

97. Karato, S.-i. Seismic anisotropy of the earth's inner core resulting from flow induced by maxwell stresses. *Nature* **402**, 871–873 (1999).

98. Buffett, B. A. & Bloxham, J. Deformation of earth's inner core by electromagnetic forces. *Geophys. research letters* **27**, 4001–4004 (2000).

99. Lasbleis, M. & Deguen, R. Building a regime diagram for the earth's inner core. *Phys. Earth Planet. Interiors* **247**, 80–93 (2015).

100. Deguen, R. & Cardin, P. Tectonic history of the earth's inner core preserved in its seismic structure. *Nat. Geosci.* **2**, 419–422 (2009).

101. Buffett, B. A. Onset and orientation of convection in the inner core. *Geophys. J. Int.* **179**, 711–719 (2009).

102. Labrosse, S. Thermal and compositional stratification of the inner core. *Comptes Rendus Geosci.* **346**, 119–129 (2014).

103. Deguen, R., Alboussiere, T. & Cardin, P. Thermal convection in earth's inner core with phase change at its boundary. *Geophys. J. Int.* **194**, 1310–1334 (2013).

104. Pozzo, M., Davies, C., Gubbins, D. & Alfè, D. Thermal and electrical conductivity of solid iron and iron–silicon mixtures at earth's core conditions. *Earth Planet. Sci. Lett.* **393**, 159–164 (2014).

105. Pourovskii, L., Mravlje, J., Pozzo, M. & Alfe, D. Electronic correlations and transport in iron at earth's core conditions. *Nat. communications* **11**, 4105 (2020).

106. Gubbins, D., Alfe, D. & Davies, C. Compositional instability of earth's solid inner core. *Geophys. Res. Lett.* **40**, 1084–1088 (2013).

107. Aubert, J., Amit, H., Hulot, G. & Olson, P. Thermochemical flows couple the earth's inner core growth to mantle heterogeneity. *Nature* **454**, 758–761 (2008).

108. Davies, C. J. & Mound, J. E. Mantle-induced temperature anomalies do not reach the inner core boundary. *Geophys. J. Int.* **219**, S21–S32 (2019).

109. Deguen, R., Alboussière, T. & Labrosse, S. Double-diffusive translation of earth's inner core. *Geophys. J. Int.* **214**, 88–107 (2018).

110. Deguen, R. & Cardin, P. Thermochemical convection in earth's inner core. *Geophys. J. Int.* **187**, 1101–1118 (2011).

111. Alboussiere, T., Deguen, R. & Melzani, M. Melting-induced stratification above the earth's inner core due to convective translation. *Nature* **466**, 744–747 (2010).

112. Monnereau, M., Calvet, M., Margerin, L. & Souriau, A. Lopsided growth of earth's inner core. *Science* **328**, 1014–1017 (2010).

113. Deguen, R., Cardin, P., Merkel, S. & Lebensohn, R. A. Texturing in earth's inner core due to preferential growth in its equatorial belt. *Phys. Earth Planet. Interiors* **188**, 173–184 (2011).

114. Buffett, B. & Wenk, H.-R. Texturing of the earth's inner core by maxwell stresses. *Nature* **413**, 60–63 (2001).

115. Deguen, R. Structure and dynamics of Earth's inner core. *Earth Planet. Sci. Lett.* **333**, 211–225 (2012).

116. Deuss, A. Normal mode constraints on shear and compressional wave velocity of the earth's inner core. *Earth Planet. Sci. Lett.* **268**, 364–375 (2008).

117. Lin, J.-F. *et al.* Sound velocities of iron-nickel and iron-silicon alloys at high pressures. *Geophys. Res. Lett.* **30** (2003).

118. Antonangeli, D. *et al.* Composition of the Earth's inner core from high-pressure sound velocity measurements in Fe–Ni–Si alloys. *Earth Planet. Sci. Lett.* **295**, 292–296 (2010).

119. Grechnev, G., Ahuja, R. & Eriksson, O. Magnetic susceptibility of hcp iron and the seismic anisotropy of earth's inner core. *Phys. Rev. B* **68**, 064414 (2003).

120. Sun, S. *et al.* Superionic effect and anisotropic texture in earth's inner core driven by geomagnetic field. *Nat. Commun.* **14**, 1656 (2023).

121. Aubert, J., Labrosse, S. & Poitou, C. Modelling the palaeo-evolution of the geodynamo. *Geophys. J. Int.* **179**, 1414–1428 (2009).

122. Davies, C. J. *et al.* Dynamo constraints on the long-term evolution of earth's magnetic field strength. *Geophys. J. Int.* **228**, 316–336 (2022).

123. Zhou, T. *et al.* Early cambrian renewal of the geodynamo and the origin of inner core structure. *Nat. communications* **13**, 1–7 (2022).

124. Lloyd, S. J., Biggin, A. J., Paterson, G. A. & McCausland, P. J. Extremely weak early cambrian dipole moment similar to ediacaran: Evidence for long-term trends in geomagnetic field behaviour? *Earth Planet. Sci. Lett.* **595**, 117757 (2022).

125. Lloyd, S. J., Biggin, A. J., Halls, H. & Hill, M. J. First palaeointensity data from the cryogenian and their potential implications for inner core nucleation age. *Geophys. J. Int.* **226**, 66–77 (2021).

126. Zhang, Y., Swanson-Hysell, N. L., Avery, M. S. & Fu, R. R. High geomagnetic field intensity recorded by anorthosite xenoliths requires a strongly powered late mesoproterozoic geodynamo. *Proc. Natl. Acad. Sci.* **119**, e2202875119 (2022).

127. Christensen, U. R. & Aubert, J. Scaling properties of convection-driven dynamos in rotating spherical shells and application to planetary magnetic fields. *Geophys. J. Int.* **166**, 97–114 (2006).

128. Tassin, T., Gastine, T. & Fournier, A. Geomagnetic semblance and dipolar–multipolar transition in top-heavy double-diffusive geodynamo models. *Geophys. J. Int.* **226**, 1897–1919 (2021).